Anomalous heat equation in a system connected to thermal reservoirs

Priyanka,[*] Aritra Kundu,[†] Abhishek Dhar,[‡] and Anupam Kundu[§]
International Centre for Theoretical Sciences, Tata Institute of Fundamental Research, Bengaluru 560089, India

(Received 27 March 2018; revised manuscript received 7 September 2018; published 2 October 2018)

We study anomalous transport in a finite one-dimensional system with two conserved quantities in the presence of thermal baths. In this system we derive exact expressions of the temperature profile and the two-point correlations in steady state as well as in the nonstationary state where the latter describe the relaxation to the steady state. In contrast to the Fourier heat equation in the diffusive case, here we show that the evolution of the temperature profile is governed by a nonlocal anomalous heat equation. We provide numerical verifications of our results.

DOI: 10.1103/PhysRevE.98.042105

I. INTRODUCTION

Transport of energy across an extended system is a paradigm of the vast class of nonequilibrium phenomena. At a macroscopic level this phenomena is often described by the phenomenological Fourier's law, which relates the energy current density $j(x,t)$ to the gradient of the temperature field $T(x,t)$: $j = -\kappa\, \partial_x T$, where κ is the thermal conductivity. This law implies diffusive energy flow across the system described by the Fourier heat equation

$$\partial_t T(x,t) = D\, \partial_x^2 T(x,t), \tag{1}$$

where $D = \kappa/c$. (For simplicity we assume κ and the specific heat c to be independent of temperature.) This equation is widely used in experiments to understand the spreading of local energy perturbations in equilibrium as well as the nonequilibrium dynamics of systems connected to reservoirs.

Surprisingly, several theoretical [1–3], numerical, as well as experimental studies [4] suggest that in many one- and two-dimensional systems heat transfer is anomalous in the sense that Fourier's law is not valid [5–7]. This phenomenon is usually manifested by several interesting features, such as divergence of thermal conductivity κ with system size L as $\kappa \sim L^{\alpha}$; $0 < \alpha < 1$, power-law decay of the equilibrium current-current autocorrelations, superdiffusive spreading of local energy perturbations, nonlinear stationary temperature profiles (even for small temperature differences), and the presence of boundary singularities in these profiles [1,6–14]. Similar nonlinear temperature profiles have been observed in simulations of realistic models of nanoscale systems [15–17]. Apart from the context of heat conduction, anomalous behavior is observed widely in a variety of physical systems, for example, in the evolution of ultracold atoms in an optical lattice [18,19], in the statistics of bird flights [20,21], in the diffusion of lipid granules inside living yeast cells [22,23], in light transmission through random media [24,25], and in various engineering applications [26–28].

There is currently no general framework to describe and explain anomalous heat transport. Recently, the theory of nonlinear fluctuating hydrodynamics has been remarkably successful in predicting anomalous scaling of dynamical correlations of conserved quantities in one-dimensional Hamiltonian systems and the corresponding slow decay of the equilibrium current-current autocorrelations [2,3,29,30]. This approach provides diverging thermal conductivity (via Green-Kubo formula) as well as Lévy scaling for the spreading of local energy perturbation. On the rigorous side, computations were done for a model of harmonic chain whose Hamiltonian dynamics was supplemented by a stochastic part that kept the conservation laws (number, energy, momentum) intact; we refer to this model as the harmonic chain momentum exchange (HCME) model. For the infinite HCME system it was shown exactly that the energy current autocorrelation has a $\sim t^{-1/2}$ decay [31]. It was also shown that, in contrast to Eq. (1), the evolution of an initially localized energy perturbation satisfied a nonlocal fractional diffusion equation $\partial_t e(x,t) = -c(-\Delta)^{3/4} e(x,t)$, where $e(x,t)$ is the energy perturbation and c is some constant [12–14,32]. The fractional Laplacian operator $(-\Delta)^{3/4}$ in the infinite space is defined by its Fourier spectrum: $|q|^{3/2}$ whereas the same for the normal Laplacian operator $-\Delta \equiv -\partial_x^2$ is q^2. In real space the $(-\Delta)^{3/4}$ operator is nonlocal [33,34]. In the framework of nonlinear fluctuating hydrodynamics [3,29], one finds that energy fluctuations spread superdiffusively, and this provides an understanding of the origin of the nonlocality.

While all these studies consider transport in *isolated* systems, quite often the transport setup in an experiment consists of an extended system connected at the two ends to heat baths at different temperatures. For diffusive systems Eq. (1) continues to describe both nonequilibrium steady state (NESS) and time-dependent properties in this setup. It is then natural to ask, what would be the corresponding evolution equation for the temperature profile in the case of anomalous transport in the experimental setup? A major problem that now arises follows from the fact that the fractional Laplacian is a nonlocal operator and so extending its definition to a finite domain is nontrivial. Several studies have addressed this issue, using

[*]priyanka@icts.res.in
[†]aritrak@icts.res.in
[‡]abhishek.dhar@icts.res.in
[§]anupam.kundu@icts.res.in

a phenomenological approach, in the context of Levy walks and Levy flights in finite domains [35,36]. It is thus crucial to have examples of specific microscopic models of systems exhibiting anomalous transport, for which the time-evolution equation in an open system setup can be derived analytically, and where one can see the nonlocal and fractional equation forms explicitly. This is the main aim of this paper.

Such attempts have recently been made in [37–39] where the problem of nonlinear steady state temperature profiles and their time evolution in the HCME model were addressed. The specific model studied was a harmonic chain of N particles where, in addition to the Hamiltonian dynamics, the momenta of nearest neighborhood particles is exchanged randomly at a constant rate γ. The chain is attached to two Langevin baths at the two ends at temperatures T_ℓ and T_r. This system has three conserved fields: the stretch $r_i = q_{i+1} - q_i$ (where q_i, $i = 1, \ldots, N$ are the particle positions), the momentum p_i, and the energy $\epsilon_i = p_i^2/2 + r_i^2/2$. This system shows anomalous current behavior $j \sim N^{-1/2}$ as well as exhibits a nonlinear stationary temperature profile $T_i = \langle p_i^2/2\rangle_{ss} = \mathcal{T}(i/N)$, which was computed analytically for fixed and free boundary conditions—surprisingly, the temperature profile was different for these cases [37,39]. The evolution of the nonstationary temperature profile $\mathcal{T}(x,\tau)$ (where $x = i/N$ and $\tau = t/N^{3/2}$ is the rescaled time) to the NESS profile was also studied [40], whereby eliminating the fast variables it was shown that $\mathcal{T}(x,\tau)$ satisfies an energy continuity equation. From an analysis of this equation it was noted that the evolution appears to be similar to the fractional diffusion equation. However, so far this has not been clearly established and in particular, an explicit representation of the corresponding fractional evolution operator is not known. In this paper, we look at a simpler model of anomalous transport in one dimension where we derive the corresponding fractional evolution equation for the temperature profile inside a finite domain and show explicitly how this evolution approaches the appropriate fractional diffusion operator in the infinite domain.

II. HARMONIC CHAIN WITH VOLUME EXCHANGE: DEFINITION OF THE MODEL AND SUMMARY OF RESULTS

This model consists of a finite one-dimensional lattice of L sites where each site carries a "stretch" variable η_i, $i = 1, 2, \ldots, L$ under an onsite external potential $V(\eta_i) = \eta_i^2/2$. The lattice is attached to two thermal reservoirs at temperatures T_ℓ and T_r on the left and right ends, respectively, and subjected to a volume-conserving stochastic noise. The dynamics of this model has two parts: (a) the usual deterministic part plus the Langevin terms coming from the baths and (b) a stochastic exchange part where ηs from any two neighboring sites, chosen at random, are exchanged at constant rate γ. The dynamics is given by

$$\begin{aligned}\frac{d\eta_i}{dt} =\ & V'(\eta_{i+1}) - V'(\eta_{i-1}) \\ & + \delta_{i,1}(-\lambda V'(\eta_1) + \sqrt{2\lambda T_\ell}\zeta_\ell(t)) \\ & + \delta_{i,L}(-\lambda V'(\eta_L) + \sqrt{2\lambda T_r}\zeta_r(t)) \\ & + \text{stochastic exchange at rate } \gamma, \end{aligned} \tag{2}$$

with fixed boundary conditions (BCs) $\eta_0 = \eta_{L+1} = 0$. Here $\zeta_{\ell,r}(t)$ are mean zero and unit variance, independent Gaussian white noises. Note that in contrast to the HCME case, this dynamics has two conserved quantities: the "volume" η_i and the energy $V(\eta_i)$. This model was first introduced by Bernardin and Stoltz in the closed system setup [13], where starting from the harmonic chain with the Hamiltonian given earlier, they have treated the positions q_is and the momenta p_is on the same footing. Note that for a harmonic chain, the dynamics of the "stretch" variable $r_i = q_{i+1} - q_i$ and the momentum variable are similar: $\dot{r}_i = p_{i+1} - p_i$ and $\dot{p}_i = r_{i+1} - r_i$ for $i = 1, 2, \ldots, N$. Hence for $N = L/2$, defining $\eta_{2j-1} = r_j$ and $\eta_{2j} = p_j$, one finds that both the above equations can be expressed in a single equation: $\dot{\eta}_m = \eta_{m+1} - \eta_{m-1}$ for $m = 1, 2, \ldots, L$. The system can also be interpreted as a fluctuating interface where the algebraic volume of the interface at site m is given by η_m and the energy $V(\eta) = \eta^2/2$ [13]. Hence, the stochastic exchange part in Eq. (2) can be thought of as a volume-energy conserving noise. We call this model a "harmonic chain with volume exchange" (HCVE).

It has been shown that the HCVE model defined on an isolated infinite one-dimensional lattice [i.e., $\lambda = 0$ in Eq. (2) with $i = -\infty, .., -1, 0, 1, .., \infty$] exhibits superdiffusion of energy [32]:

$$\begin{aligned}&\partial_t e(x,t) = -\mathbb{L}_\infty[e(x,t)], \\ &\mathbb{L}_\infty = \frac{1}{\sqrt{2\gamma}}[(-\Delta)^{3/4} - \nabla(-\Delta)^{1/4}],\end{aligned} \tag{3}$$

where the skew-fractional operator $\mathbb{L}_\infty$ has the Fourier representation $|q|^{3/2}[1 - i\ \mathrm{sgn}(q)]$ with $i = \sqrt{-1}$ and $\mathrm{sgn}(q)$ is the signum function. Note that the spectrum is different from that in the infinite HCME model. In this paper, however, we consider the HCVE model on a finite lattice of size L in open setup, i.e., connected to heat baths at the two ends as described in Eq. (2). It is known that in this case also, as in HCME, the stationary current scales as $j \sim L^{-1/2}$ [32].

Results. We explicitly find that in the large-L limit the average energy current $j = -2\langle\eta_i\eta_{i+1}\rangle - \gamma(\langle\eta_{i+1}^2\rangle - \langle\eta_i^2\rangle)$ in the stationary state is given by

$$j_{ss} = \frac{1}{2}\sqrt{\frac{\pi}{\gamma}}\frac{(T_\ell - T_r)}{\sqrt{L}} + O\left(\frac{1}{L}\right). \tag{4}$$

In the nonstationary regime, we numerically find that the temperature profile $T_i(t) = \langle\eta_i^2(t)\rangle$ and the two-point correlations $C_{i,j}(t) = \langle\eta_i(t)\eta_j(t)\rangle$ for $i \neq j$ have the following scaling forms:

$$\begin{aligned}T_i(t) &= \mathcal{T}\left(\frac{i}{L}, \frac{t}{L^{3/2}}\right), \\ C_{i,j}(t) &= \frac{1}{\sqrt{L}}\mathcal{C}\left(\frac{|i-j|}{\sqrt{L}}, \frac{i+j}{2L}, \frac{t}{L^{3/2}}\right),\end{aligned} \tag{5}$$

in the leading order for large L. The scaling functions $\mathcal{T}(y,\tau)$ and $\mathcal{C}(x,y,\tau)$ satisfy the following equations inside the

domain $\mathcal{D} = \{0 \leqslant x \leqslant \infty\,;\, 0 \leqslant y \leqslant 1\}$:

$$\partial_y \mathcal{C}(x, y, \tau) = -\gamma\, \partial_x^2 \mathcal{C}(x, y, \tau), \tag{6}$$

$$\partial_y \mathcal{T}(y, \tau) = -2\gamma [\partial_x \mathcal{C}(x, y, \tau)]_{x=0}, \tag{7}$$

$$\partial_\tau \mathcal{T}(y, \tau) = 2\partial_y \mathcal{C}(0, y, \tau), \tag{8}$$

with $\mathcal{C}(x, y, 0)|_{x\to\infty} = 0$ and $\mathcal{C}(x, y, 0) = 0$. We find that the exact solutions of these equations are given by

$$\mathcal{T}(y, \tau) = \mathcal{T}_{ss}(y) + \mathcal{T}_r(z = 1 - y, \tau), \tag{9}$$

$$\mathcal{C}(x, y, \tau) = \mathcal{C}_{ss}(x, y) + \mathcal{C}_r(x, z = 1 - y, \tau). \tag{10}$$

In the above equation, the NESS parts of the profiles are

$$\begin{aligned} \mathcal{T}_{ss}(y) &= T_r + (T_\ell - T_r)\sqrt{1 - y}, \\ \mathcal{C}_{ss}(x, y) &= -\frac{T_\ell - T_r}{4}\sqrt{\frac{\pi}{\gamma}}\,\mathrm{erfc}\left(\frac{x}{\sqrt{4\gamma(1-y)}}\right). \end{aligned} \tag{11}$$

The relaxation parts to the above steady states are given as

$$\mathcal{C}_r(x, z, \tau) = -\int_0^z \frac{\exp\left(-\frac{x^2}{4\gamma(z-z')}\right)}{\sqrt{4\pi\gamma(z-z')}}\,\frac{\partial \mathcal{T}_r(z', \tau)}{\partial z'} dz', \tag{12}$$

where $\mathcal{T}_r(z, \tau)$ satisfies the following continuity equation:

$$\partial_\tau \mathcal{T}_r(z, \tau) = \frac{1}{\sqrt{\pi\gamma}}\partial_z\left[\int_0^z dz'\,\frac{\partial_{z'}\mathcal{T}_r(z', \tau)}{\sqrt{z - z'}}\right], \tag{13}$$

inside the domain $0 \leqslant z \leqslant 1$ with BCs $\mathcal{T}_r(0, \tau) = \mathcal{T}_r(1, \tau) = 0$. The relaxation parts $\mathcal{T}_r(z, \tau)$ and $\mathcal{C}_r(x, z, \tau)$ describe the approach towards the NESS solutions in the $\tau \to \infty$ limit. Note that Eq. (13) can formally be written in terms of the Riemann-Liouville operator. Equations (4), (11), (12), and (13), comprise our main results. The evolution of the temperature in Eq. (13) is indeed given by a linear but nonlocal equation defined inside a finite domain $0 \leqslant z \leqslant 1$. However, following a similar calculation for the infinite system we later show that Eq. (13) reduces to Eq. (3) in Sec. III. This establishes, without ambiguity, that the nonlocal operator in Eq. (13) is the correct finite domain representation of the fractional operator $\mathbb{L}_\infty$ in Eq. (3). Another point to note is that the temperature profile in SS, $\mathcal{T}_{ss}(y)$, is asymmetric under space reversal as the microscopic model itself does not have such symmetry. As a result, any locally created perturbation splits into one traveling sound mode and one nonmoving heat mode. This is in contrast to the HCME model, where one observes two sound modes moving in opposite directions in addition to a nonmoving heat mode [13,29]. Consequently, in this case there is singularity in $\partial_y \mathcal{T}_{ss}(y)$ only at one boundary and we find that the meniscus exponent [41] is again $1/2$ as in the HCME model with fixed boundary conditions. Interestingly, it turns out that for this boundary condition, both the temperature and the correlation become independent of the strength of coupling λ with the heat baths in the large L limit.

III. DERIVATION OF THE RESULTS

A. The Fokker-Planck operator and discrete equations for correlation functions

We start with the Fokker-Planck (FP) equation associated to the dynamics Eq. (2), which describes the evolution of the joint distribution $P(\vec{\eta}, t)$ of $\vec{\eta} = (\eta_1, \eta_2, \ldots, \eta_L)$ at time t:

$$\partial_t P(\vec{\eta}, t) = [\mathcal{L}_\ell + \mathcal{L}_b + \mathcal{L}_{ex}]\, P(\vec{\eta}, t), \tag{14}$$

where $\mathcal{L}_\ell$ is the Liouvillian part, $\mathcal{L}_b$ contains the effects of the Langevin baths at the boundaries, and $\mathcal{L}_{ex}$ represents the contribution from the exchange noise. The explicit expression of the deterministic part of the FP equation given by operators $\mathcal{L}_l$, $\mathcal{L}_b$ is defined as

$$\begin{aligned} \mathcal{L}_l &= \sum_{i=2}^{L-1} [V'(\eta_{i-1}) - V'(\eta_{i+1})]\partial_{\eta_i} + V'(\eta_{L-1})\partial_{\eta_L} - V'(\eta_2)\partial_{\eta_1}, \\ \mathcal{L}_b &= \lambda T_\ell\, \partial_{\eta_1}^2 + \lambda \partial_{\eta_1} V'(\eta_1) + \lambda T_r\, \partial_{\eta_L}^2 + \lambda \partial_{\eta_L} V'(\eta_L), \end{aligned}$$

where T_ℓ and T_r are the temperatures of the reservoirs on the left and right, respectively. The stochastic part $\mathcal{L}_{ex}$ is given as

$$\mathcal{L}_{ex} = \gamma\left(\sum_{i=1}^{L-1} P(\vec{\eta}_{i,i+1}) - P(\vec{\eta})\right), \tag{15}$$

where $\vec{\eta}_{i,i+1}$ denotes the configuration after the exchange of variable i with $i + 1$. Starting from the FP equation in Eq. (14), we obtain the dynamical equations satisfied by $T_i = \langle \eta_i^2(t)\rangle$ and $C_{i,j} = \langle \eta_i(t)\eta_j(t)\rangle$ for $i \neq j$ in the bulk:

$$\begin{aligned} \dot{C}_{ij} &= C_{i+1,j} - C_{i-1,j} + C_{i,j+1} - C_{i,j-1} \\ &\quad + \gamma[C_{i-1,j} + C_{i+1,j} + C_{i,j-1} + C_{i,j+1} - 4C_{i,j}], \\ \dot{C}_{i,i+1} &= T_{i+1} - C_{i-1,i+1} + C_{i,i+2} - T_i \\ &\quad + \gamma[C_{i-1,i+1} + C_{i,i+2} - 2C_{i,i+1}], \\ \dot{T}_i &= 2[C_{i,i+1} - C_{i-1,i}] + \gamma[T_{i+1} + T_{i-1} - 2T_i]. \end{aligned} \tag{16}$$

The rest of the equations at the boundaries are given in Appendix. Fortunately, the equations for two-point correlations do not involve higher-order correlations, which allows us to solve these equations analytically, in the $L \to \infty$ limit.

B. Derivation of continuum equations for the temperature and correlation fields from the discrete equations

In this section, we outline the steps to obtain the continuum set of partial differential equations (PDEs), Eqs. (6)–(8). We first solve the discrete equations numerically to observe that for large L the solutions have the scaling properties as given in Eq. (5), where we have two length scales of $O(L)$ along the diagonal ($i + j =$ constant) and of $O(\sqrt{L})$ along perpendicular to the diagonal ($|i - j| =$ constant) direction, and a timescale of $O(L^{3/2})$. This timescale can be anticipated from the propagator $e^{-|q|^{3/2}[1 - i\,\mathrm{sgn}(q)]t}$ of Eq. (3) in Fourier space. The two length scales are understood by looking at the orders of the $C_{i,j}$ and T_i, and their derivatives numerically. Interestingly, the scaled correlation function $\mathcal{C}$ relaxes very fast over a much shorter timescale $[O(L)]$ compared to the

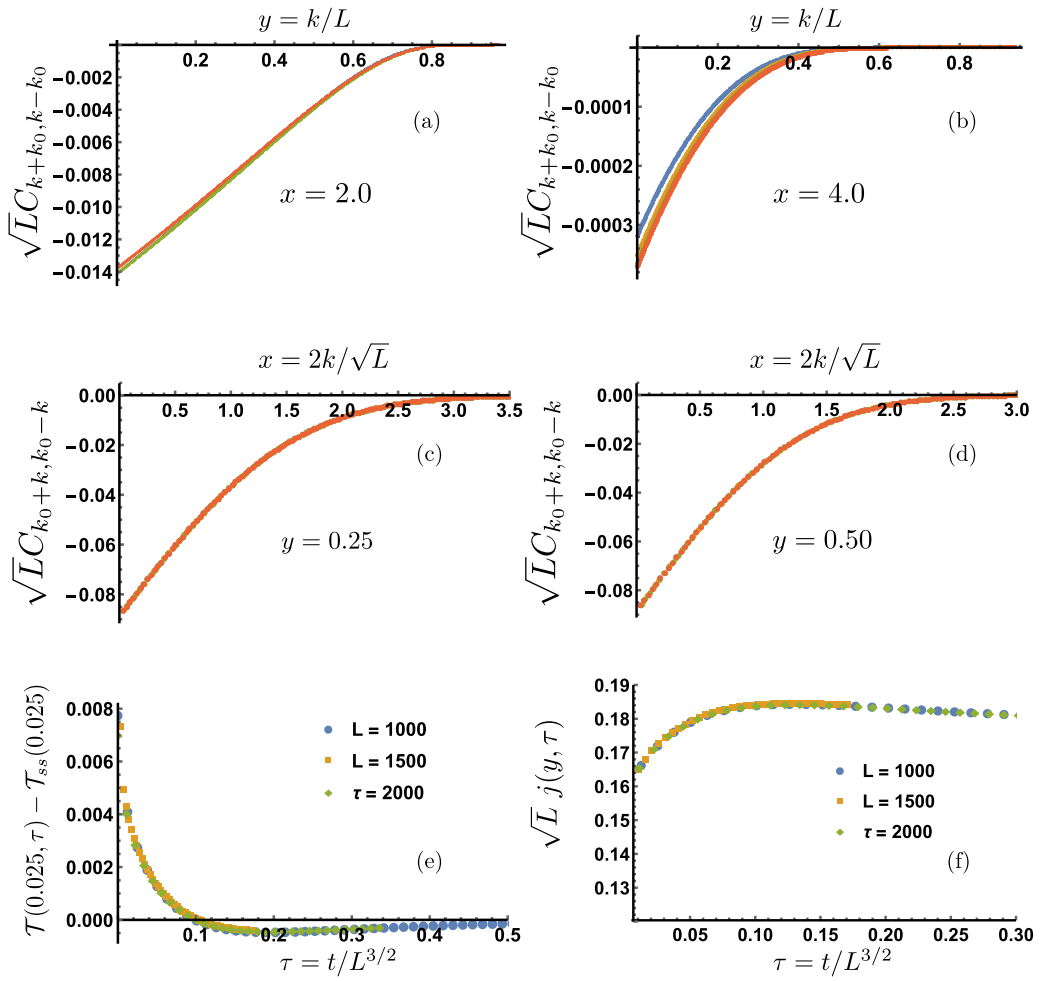

FIG. 1. Data collapse of the correlation functions and temperature profile confirming the scaling behaviors in Eqs. (17) and (18). (a, b) The data collapse as a function of the scaling variable $y = (i + j)/2L$ with four systems sizes $L = 1000$ (blue, dark gray), $L = 2000$ (orange, deep gray), $L = 3000$ (green, light gray), and $L = 4000$ (red, bottom dark gray), for two fixed values of $x = |j - i|/\sqrt{L}$. (c, d) The data collapse as a function of the scaling variable x with the above four system sizes for two fixed values of y. The collapse is so good that other colors and shades are not visible. (e) The scaling behavior for the evolution of the temperature $\mathcal{T}(y,\tau) = T_{\lfloor yL \rfloor}(\tau L^{3/2})$ at a fixed position $y = 0.025$ for different system sizes as a function of the scaled time $\tau = t/L^{3/2}$. Note that the temperatures are of $O(1)$ whereas the correlations are of $O(1/\sqrt{L})$. Also note from figures (c) and (b) that $\mathcal{C}_{ss}(x \to \infty, z) = 0$. (f) Establishes that the current in the system is of order $1/\sqrt{L}$ and also evolves in scaled time $\tau = t/L^{3/2}$. The other parameters in the simulation are $\gamma = \Lambda = 1$, $T_\ell = 1.1$, $T_r = 0.9$.

evolution timescale $[O(L^{3/2})]$ of the temperature field $\mathcal{T}$. Due to this fact, Eqs. (6) and (7) do not involve the time derivative. As a result, the correlation function $\mathcal{C}$ evolves adiabatically, obeying the (anti-)diffusion Eq. (6), with a drive at the boundary by the time-dependent temperature field through Eq. (7). The equation for the temperature profile given in Eq. (8) is in the expected continuity equation.

These observations suggest that we look for solutions of Eq. (16) in the scaling form Eq. (5). In the nonstationary regime, we numerically find that the temperature profile $T_i(t) = \langle \eta_i(t)^2 \rangle$ and the two-point correlations $C_{i,j}(t) = \langle \eta_i(t)\eta_j(t) \rangle$ for $i \neq j$ have the following scaling forms,

$$C_{i,j}(t) = \frac{1}{\sqrt{L}}\mathcal{C}\left(\frac{|i-j|}{\sqrt{L}}, \frac{i+j}{2L}, \frac{t}{L^{3/2}}\right), \tag{17}$$

$$T_i(t) = \mathcal{T}\left(\frac{i}{L}, \frac{t}{L^{3/2}}\right), \tag{18}$$

in the leading order for large L which are also supported by numerical evidence shown in Fig. 1. In Figs. 1(a)–1(d) we verify the scaling behaviors of the correlations in Eq. (17). Figures 1(c) and 1(d) describe scaling behavior with respect to time. Using these, we define continuum ordinates as $\frac{|i-j|}{\sqrt{L}} = x$, $\frac{|i+j|}{2L} = y$, $\frac{t}{L^{3/2}} = \tau$, and $\frac{1}{\sqrt{L}} = \epsilon$, where $x \in (0, \infty)$ and $y \in (0, 1)$. In the following, we insert this scaling form and Taylor expand in $\epsilon = 1/\sqrt{L}$. Keeping terms to leading order in ϵ we obtain the continuum equations.

1. **Bulk Equations, $|i - j| \geqslant 2$**

The discrete equation in bulk:

$$\dot{C}_{i,j} = -\big(C_{i-1,j} - C_{i+1,j} + C_{i,j-1} - C_{i,j+1} - \gamma[C_{i,j-1} + C_{i,j+1} + C_{i+1,j} + C_{i-1,j} - 4C_{i,j}]\big), \tag{19}$$

using above scaling definitions, we can write the above-mentioned discrete equation as

$$\epsilon^4\partial_\tau\mathcal{C}(x,y,\tau) = -\epsilon\Big\{\mathcal{C}\Big(x-\epsilon,y-\frac{\epsilon^2}{2}\Big)-\mathcal{C}\Big(x+\epsilon,y+\frac{\epsilon^2}{2}\Big)+\mathcal{C}\Big(x+\epsilon,y-\frac{\epsilon^2}{2}\Big)-\mathcal{C}\Big(x-\epsilon,y+\frac{\epsilon^2}{2}\Big) -\gamma\Big[\mathcal{C}\Big(x+\epsilon,y-\frac{\epsilon^2}{2}\Big)+\mathcal{C}\Big(x-\epsilon,y+\frac{\epsilon^2}{2}\Big)+\mathcal{C}\Big(x+\epsilon,y+\frac{\epsilon^2}{2}\Big)+\mathcal{C}\Big(x-\epsilon,y-\frac{\epsilon^2}{2}\Big)-4\mathcal{C}(x,y)\Big]\Big\}, \tag{20}$$

which by Taylor expansion of each term in x, y, and τ, we obtain the leading-order terms for the continuum dynamical equation as

$$\epsilon^4\partial_\tau\mathcal{C}(x,y,\tau) = 2\epsilon^3\partial_y\mathcal{C}(x,y,\tau)+2\gamma\epsilon^3\partial_x^2\mathcal{C}(x,y,\tau). \tag{21}$$

At the dominant order ($O(\epsilon^3)$), we find

$$\partial_y\mathcal{C}(x,y,\tau)+\gamma\partial_x^2\mathcal{C}(x,y,\tau) = 0. \tag{22}$$

2. **Nearest-neighbor term, $j = i+1$**

The off-diagonal term,

$$\dot{C}_{i,i+1} = T_{i+1}-C_{i-1,i+1}+C_{i,i+2}-T_i +\gamma[C_{i-1,i+1}+C_{i,i+2}-2C_{i,i+1}], \tag{23}$$

after proper scaling, we get,

$$\epsilon^4\partial_\tau\mathcal{C}\Big(\epsilon,y+\frac{\epsilon^2}{2},\tau\Big) = \mathcal{T}(y+\epsilon^2)-\mathcal{T}(y)+\epsilon\mathcal{C}(2\epsilon,y+\epsilon^2)-\epsilon\mathcal{C}(2\epsilon,y) +\gamma\epsilon[\mathcal{C}(2\epsilon,y)+\mathcal{C}(2\epsilon,y+\epsilon^2)-2\mathcal{C}(\epsilon,y+\epsilon^2/2)].$$

Expanding the above equation in x and y, and keeping the relevant order terms in ϵ we get the continuum equation as

$$\epsilon^4\partial_\tau\mathcal{C}(0,y,\tau) = \epsilon^2[\partial_y\mathcal{T}(y,\tau)+2\gamma\partial_x\mathcal{C}(0,y,\tau)]+O(\epsilon^3), \tag{24}$$

and hence to the dominating order, the governing continuum equation is

$$\partial_y\mathcal{T}(y,\tau)+2\gamma\partial_x\mathcal{C}(0,y,\tau) = 0. \tag{25}$$

3. **Diagonal term $i = j$**

Next is the diagonal term where $i = j$,

$$\dot{T}_i = 2[C_{i,i+1}-C_{i-1,i}]+\gamma[T_{i+1}+T_{i-1}-2T_i], \tag{26}$$

which in continuum limit given as

$$\epsilon^3\partial_\tau\mathcal{T}(y,\tau) = 2\epsilon\Big[\mathcal{C}\Big(\epsilon,y+\frac{\epsilon^2}{2}\Big)-\mathcal{C}\Big(\epsilon,y-\frac{\epsilon^2}{2}\Big)\Big] +\gamma\big[\mathcal{T}(y+\epsilon^2)+\mathcal{T}(y-\epsilon^2)-2\mathcal{T}(y)\big].$$

After expansion, we arrive at

$$\epsilon^3\partial_\tau\mathcal{T}(y,\tau) = 2\epsilon\Big[\epsilon^2\partial_y\mathcal{C}(0,y,\tau)+\epsilon^3\frac{\gamma}{2}\partial_y^2\mathcal{T}(y,\tau)\Big] +O(\epsilon^4). \tag{27}$$

Hence, the leading-order term is

$$\partial_\tau\mathcal{T}(y,\tau) = 2\partial_y\mathcal{C}(0,y,\tau). \tag{28}$$

4. **Current**

The microscopic energy current in the system is defined through

$$\partial_t\langle\eta_i^2\rangle = -[j_{i\to i+1}-j_{i-1\to i}], \tag{29}$$

where $j_{i\to i+1} = -2C_{i,i+1}-\gamma(T_{i+1}-T_i)$. The stochastic part of the current decays as $O(1/L)$ and in the macroscopic limit goes to zero. In the continuum limit, the deterministic part contributes in the leading order to provide $j = -2\mathcal{C}(0,y,\tau)/\sqrt{L}$.

The above analysis gives us the bulk equations for the system as given in Eqs. (6)–(8). Solutions of these equations for $\mathcal{C}(x,y,\tau)$ and $\mathcal{T}(y,\tau)$ have two parts, Eq. (10). It is easier to deal with these equations with the transformation of $z = 1-y$, which satisfies

$$\partial_z\mathcal{C}(x,z,\tau) = \gamma\partial_x^2\mathcal{C}(x,z,\tau)\,, \tag{30}$$

$$\partial_z\mathcal{T}(z,\tau) = 2\gamma\partial_x\mathcal{C}(x,z,\tau)_{x=0}\,, \tag{31}$$

$$\partial_\tau\mathcal{T}(y,\tau) = -2\partial_z\mathcal{C}(0,z,\tau). \tag{32}$$

These equations have to be solved with appropriate boundary conditions which will be discussed in the next few sections, where we discuss the solution of these equations in steady state and the approach to it.

C. Stationary state solution of $\mathcal{T}(z)$ and $\mathcal{C}(x,z)$

In the NESS the equations (30)–(32) become simpler, since $\partial_\tau\mathcal{T}\to 0$ as $\tau\to\infty$, implying $\mathcal{C}_{ss}(0,y) = d$. Now making the variable transformation $z = (1-y)$, the problem of finding $\mathcal{C}_{ss}$ reduces to solving a diffusion equation with its value at $x = 0$ held fixed for all y. We need to solve these equations along with the boundary conditions,

$$(i)\,\mathcal{C}_{ss}(x,z\to 0) = 0,\ (ii)\,\mathcal{C}_{ss}(x\to\infty,z) = 0,$$
$$(iii)\,\mathcal{C}_{ss}(x=0,z) = d. \tag{33}$$

The boundary conditions (i) and (ii) follow from our numerical observations shown in Figs. 1(a,b) and Figs. 1(c,d), respectively. The last boundary condition (iii) is obtained by observing that the left-hand side of (32) is zero in the steady state; hence $[\partial_z\mathcal{C}_{ss}(0,z) = 0]$. The unknown constant d will be fixed by the temperatures at the boundary. The first equation is easy to solve by taking the Laplace transform in z along with boundary conditions. Finally, after inverting the Laplace transform, we find the solution is given by

$$\mathcal{C}_{ss}(x,z) = d\ \mathrm{erfc}\Big[\frac{x}{\sqrt{4\gamma z}}\Big], \tag{34}$$

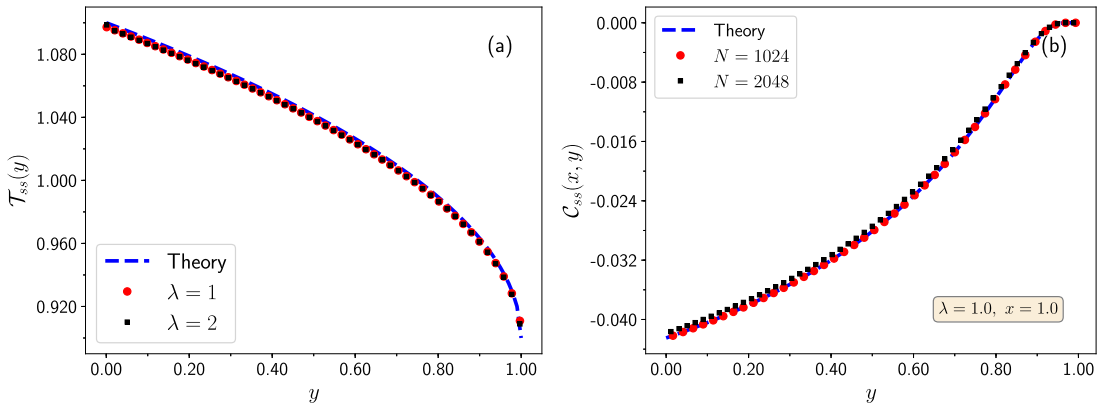

FIG. 2. Numerical verification of the analytical NESS predictions for (a) $\mathcal{T}_{ss}(y)$ and (b) $\mathcal{C}_{ss}(x, y)$ in Eq. (11). Symbols denote corresponding quantities that are obtained from simulations with $\omega = \gamma = 1$, $T_\ell = 1.1$, $T_r = 0.9$, and $N = 1024$, whereas the dashed lines are from theory.

where erfc is the complimentary error function defined as $\mathrm{erfc}(x) = 1 - \frac{2}{\sqrt{\pi}} \int_0^x dt e^{-t^2}$. Now, using this solution in Eq. (31), we get $\partial_z \mathcal{T}_{ss}(z) = -d\sqrt{4\gamma/\pi z}$, whose solution is

$$\mathcal{T}_{ss}(z) = \mathcal{T}_{ss}(0) - 2d\sqrt{\frac{4\gamma z}{\pi}}. \tag{35}$$

The constants $\mathcal{T}_{ss}(0)$ and d will now be determined from the boundary conditions of the temperature field, $\mathcal{T}(z = 0) = T_r$ and $\mathcal{T}(z = 1) = T_\ell$. We finally have

$$T_\ell - T_r = -2d\sqrt{\frac{4\gamma}{\pi}}, \quad d = -\frac{\Delta T}{4}\sqrt{\frac{\pi}{\gamma}}, \tag{36}$$

where $\Delta T = (T_\ell - T_r)$ is the temperature difference between the left and right heat baths. Reverting now back to y variables using $z = 1 - y$, the exact expressions for the steady-state temperature profile and correlations are

$$\mathcal{T}_{ss}(y) = T_r + \Delta T\sqrt{1 - y}, \tag{37}$$

$$\mathcal{C}_{ss}(x, y) = -\frac{\Delta T}{4}\sqrt{\frac{\pi}{\gamma}}\,\mathrm{erfc}\left[\frac{x}{\sqrt{4\gamma(1 - y)}}\right]. \tag{38}$$

Hence the current in the system is given by $j_{ss} = \frac{\mathcal{J}_{ss}}{\sqrt{L}}$, where,

$$j_{ss} = -\frac{2\mathcal{C}_{ss}(0, y)}{\sqrt{L}} = \frac{\Delta T}{2}\sqrt{\frac{\pi}{\gamma}}\frac{1}{\sqrt{L}}. \tag{39}$$

In Fig. 2 we verify the analytical results for $\mathcal{T}_{ss}$ and $\mathcal{C}_{ss}$ numerically, where we observe nice agreement. Next, we study the solution in the relaxation regime.

D. Relaxation to steady state

We now focus on the relaxation to the NESS. It is often convenient to separate the relaxation part as done in Eqs. (9) and (10), where $\mathcal{T}_r(z, \tau)$ and $\mathcal{C}_r(x, z, \tau)$ describe the approach towards the NESS solutions in Eq. (11). It is easy to see that $\mathcal{C}_r(x, z, \tau)$ and $\mathcal{T}_r(z, \tau)$ satisfy the following equations:

$$\partial_z \mathcal{C}_r(x, z, \tau) = \gamma \partial_x^2 \mathcal{C}_r(x, z, \tau), \tag{40}$$

$$\partial_z \mathcal{T}_r(z, \tau) = 2\gamma[\partial_x \mathcal{C}_r(x, z, \tau)]_{x=0}, \tag{41}$$

$$\partial_\tau \mathcal{T}_r(z, \tau) = -2\partial_z \mathcal{C}_r(0, z, \tau), \tag{42}$$

with initial condition $\mathcal{C}_r(x, z, 0) = 0$ and BC $\mathcal{C}_r(x, z, \tau)|_{x\to\infty} = 0$. The above equations are obtained from Eqs. (6)–(8) after subtracting the steady-state part and then making the variable transformation $z = (1 - y)$. Note that the BC in Eq. (41) acts like a current source, at the $x = 0$ boundary, to the diffusion equation (40). The Greens function $g(x, z)$ of this equation with above BCs satisfies $\partial_z g(x, z) = \frac{\gamma}{2}\partial_x^2 g(x, z)$, where $g(x, z)$ is given by $g(x, z) = \sqrt{4\gamma z}h(x/\sqrt{4\gamma z})$, where $h(w) = \frac{e^{-w^2}}{\pi} - w\mathrm{erfc}(w)$; hence the general time-dependent solution is written as

$$\begin{aligned}\mathcal{C}_r(x, z, \tau) = &2\int_0^z dx' \frac{e^{-(x-x')^2/(4\gamma z)}}{\sqrt{4\pi\gamma z}}\mathcal{C}_r(x', 0, \tau) \\ &- \frac{1}{2\gamma}\left(\int_0^z dz'[g(x, z - z')\partial_{z'}^2 \mathcal{T}_r(z', \tau)]\right) \\ &- \frac{1}{2\gamma}\,\partial_{z'}\mathcal{T}_r(z', \tau)g(x, z)|_{z'\to 0}.\end{aligned} \tag{43}$$

With the initial condition $\mathcal{C}_r(x, 0, \tau) = 0$ the first term drops out. It is easy to check that the remaining part satisfies (40) with boundary condition (41) as follows:

$$\begin{aligned}&\partial_x \mathcal{C}_r(x, z, \tau)|_{x\to 0} \\ &= \frac{1}{2\gamma}\left(\int_0^z dz' \partial_{z'}^2 \mathcal{T}_r(z', \tau) + \partial_{z'}\mathcal{T}_r(z', \tau)|_{z'\to 0}\right) \\ &= \frac{1}{2\gamma}\partial_z \mathcal{T}_r(z, \tau),\end{aligned} \tag{44}$$

where we have used $\partial_x g(x, z)|_{x\to 0} = -1$. Further, using the fact that $g(x, z - z')\partial_{z'}\mathcal{T}_r(z')|_{z'\to z} \to 0$ we can simplify (43) as

$$\begin{aligned}\mathcal{C}_r(x, z, \tau) &= \frac{1}{2\gamma}\left(\int_0^z dz' \partial_{z'}[g(x, z - z')]\partial_{z'}\mathcal{T}_r(z', \tau)\right) \\ &= -\frac{1}{\sqrt{\gamma}}\int_0^z dz' \frac{e^{-x^2/[4\gamma(z-z')]}}{\sqrt{4\pi(z - z')}}\partial_{z'}\mathcal{T}_r(z', \tau),\end{aligned}$$

which gives the relaxation of the correlation fields. The evolution of temperature field is obtained from (42) by putting $x \to 0$ in the above expression for $\mathcal{C}_r(x, z, \tau)$, and we immediately

have

$$\partial_\tau \mathcal{T}_r(z,\tau) = \kappa\, \partial_z \int_0^z \frac{\partial_{z'}\mathcal{T}_r(z',\tau)}{\sqrt{z-z'}} dz', \quad 0 \leqslant z \leqslant 1, \tag{45}$$

where $\kappa = \frac{1}{\sqrt{\pi\gamma}}$. The infinite system generalization of this equation will be discussed later (see Sec. III E).

Series solution of the fractional PDE Eq. (45) in the finite domain. The evolution of the relaxation part of the temperature profile, i.e., $\mathcal{T}_r(1-y,\tau) = \mathcal{T}(y,\tau) - \mathcal{T}_{ss}(y)$, is given by Eq. (45). Note that $\mathcal{T}_r(z,\tau)$ is zero at both the boundaries: $z = 0$ and $z = 1$. As a result it is natural to expand this function in $\alpha_n(z) = \sqrt{2}\sin(n\pi z)$, $n = 1, 2, 3\ldots$ complete basis defined in $z \in (0,1)$ as $\mathcal{T}_r(z,\tau) = \sum_n \hat{\mathcal{T}}_n(\tau)\alpha_n(z)$. Substituting this form in Eq. (45), we have

$$\sum_n \dot{\hat{\mathcal{T}}}_n \alpha_n(z) = \kappa \sum_n \hat{\mathcal{T}}_n(\tau)(n\pi)\partial_z \int_0^z \frac{\phi_n(z')}{\sqrt{z-z'}} dz'. \tag{46}$$

Now let us expand the function $f_n(z) = \partial_z \int_0^z \frac{\phi_n(z')}{\sqrt{z-z'}} dz'$ also in orthogonal basis $\alpha_n(y)$, $n = 1, 2\ldots$. Let the expansion be given as $f_n(z) = \sum_{l=1} \zeta_{nl}\alpha_l(z)$ where $\zeta_{nl} = \int_0^1 dz\; f_n(z)\,\alpha_l(z)$. As a result we have

$$\sum_{n=1} \dot{\hat{\mathcal{T}}}_n \alpha_n(z) = \kappa \sum_{n,l=1} \hat{\mathcal{T}}_n(\tau)(n\pi)\zeta_{nl}\alpha_l(z). \tag{47}$$

Using orthogonality, this can be written in vector notation as ($\hat{\mathcal{T}}_n = \langle n|\hat{\mathcal{T}}\rangle$),

$$|\dot{\hat{\mathcal{T}}}\rangle = \kappa\, \mathbf{B}|\hat{\mathcal{T}}\rangle, \tag{48}$$

where $B_{nk} = (n\pi)\zeta_{nk}$ and $|\ldots\rangle$ denotes a column vector. If R is the matrix which diagonalizes $\mathbf{B}$ as $R^{-1}\mathbf{B}R = \Lambda$, then the time-dependent solution is given as $|\hat{\mathcal{T}}(\tau)\rangle = \mathrm{Re}^{\kappa\Lambda\tau}R^{-1}|\hat{\mathcal{T}}(0)\rangle$ and temperature at time τ is given as $\mathcal{T}(y,\tau) = \mathcal{T}_{ss}(y) + \sum_n \alpha_n(1-y)\hat{\mathcal{T}}_n(\tau)$. As the temperature field evolves at much faster timescales compared to the correlation field, the time-dependent solution for correlations $\mathcal{C}_r(x,1-y,\tau)$ is governed by the evolution of the temperature field. The solution for evolution of correlations is written as $\mathcal{C}(x,y,\tau) = \mathcal{C}_r(x,1-y,\tau) + \mathcal{C}_{ss}(x,y)$, where

$$\begin{aligned}\mathcal{C}(x,z,\tau) &= -\int_0^z dz' \frac{e^{-x^2/(4\gamma(z-z'))}}{\sqrt{4\pi\gamma(z-z')}}\partial_{z'}T_r(z',\tau),\\ &= \sum_{n=1}\hat{\mathcal{T}}_n(\tau)(n\pi)\int_0^z dz' \frac{e^{-x^2/(4\gamma(z-z'))}}{\sqrt{4\pi\gamma(z-z')}}\phi_n(z'),\end{aligned} \tag{49}$$

where $\phi_n(y) = \sqrt{2}\cos(n\pi y)$, $n \geqslant 1$, and $\phi_0(y) = 1$. The integral can be evaluated explicitly, and doing the summations gives the evolution of the correlation fields.

Eigensystem. The eigenvalues (μ_n) of the bounded skew-fractional Laplacian $\mathbf{B}$ have interesting behavior; the first four of them are real and distinct. The higher eigenvalues all come in complex conjugate pairs. For large n, $\mu_n \sim \sqrt{\frac{\pi}{2}}|n\pi|^{3/2}[1 \pm i\ \mathrm{sgn}(n)]$, but for smaller n there is a systematic deviation due to the effect of finite domain. In Fig. 3, the real and imaginary part of alternate eigenvalues are plotted as a function of n, where the asymptotic scaling with $\sqrt{\frac{\pi}{2}}(n\pi)^{3/2}$ is seen clearly for large n. We note that this is not due to the the truncation

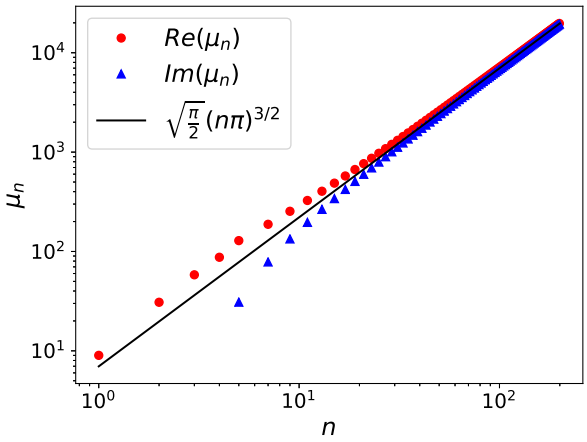

FIG. 3. The real and imaginary part of the alternate eigenvalues for matrix $\mathbf{B}$. The first four eigenvalues are completely real and distinct. The higher eigenvalue comes in pairs of $\mu_n(1 \pm i)$. For large n (plotted alternately), the eigenvalues are close to $\sqrt{\frac{\pi}{2}}(n\pi)^{3/2}(1 \pm i)$. For smaller n, there is a deviation from asymptomatic scaling due to the finite definition of the operator.

of the matrix but an artefact of the finiteness of the system. Note that the large n behavior of μ_n is similar to the Fourier spectrum of the nonlocal operator $\mathbb{L}_\infty$ in Eq. (3) describing the evolution in infinite system. Hence it is interesting to see if one recovers the evolution equation (3) in the infinite system limit Sec. III E. The eigenvectors of the operator are defined as $\psi_n(y) = \sum_{l=1} R^{-1}_{nl}\alpha_l(y)$. Numerically, computing this gives the first six eigenvectors to be completely real. The eigenvectors corresponding to higher eigenvalues are complex and come in pairs. The real and imaginary parts of the first few eigenvectors are shown in Fig. 4. In Appendix A 3, the real and the imaginary parts of the eigenvector for $n \geqslant 7$ are plotted in polar plots. For plane wave solutions these would have been circles of length 1; here the polar plot shows a spiral decay to origin owing to the skewness of the operator.

Comparison with numerics. While it is difficult to solve this infinite order matrix equation analytically, we solve it numerically by truncating it at some finite order. In Fig. 5, we compare the evolution from this numerical solution with the same obtained from direct numerical simulation of Eq. (2) and observe nice agreement. Using this solution in Eq. (12) we obtain $C(x,z,\tau)$ in Eq. (10), which we also compare with simulation results in the inset of Fig. 5 and again observe good agreement.

E. Fractional evolution of temperature in an infinite line

One can extend the calculation for temperature evolution Eq. (45) in a finite system of length L and obtain the same set of bulk equations which now holds for $y \in [0, L]$. We are interested in the behavior of the evolution of temperature profile in the $L \to \infty$ limit, where the effect of boundaries is not important. The evolution equations for the relaxation parts in this case are the same as those of Eqs. (40)–(42) but now $0 \leqslant x \leqslant \infty$ and $0 \leqslant y \leqslant L$. To proceed, we introduce the orthonormal and complete basis in $y \in [0, L]$, $\phi_n^{\pm}(y) = \frac{1}{\sqrt{L}}e^{\pm in\pi y/L}$ for $n \geqslant 1$ and $\phi_0(y) = 1/\sqrt{L}$. Expanding the

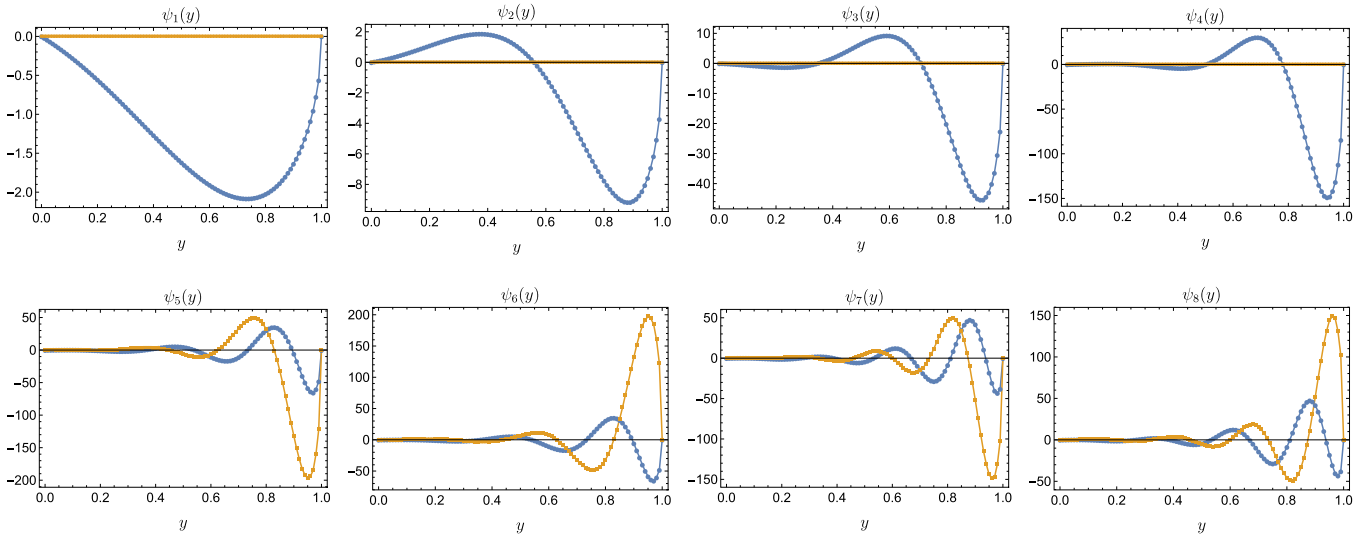

FIG. 4. The real (blue, deep gray) and imaginary (orange, light gray) part of the right eigenvectors for the matrix **B** for the first few eigenvalues. The plots for even-ordered eigenvectors ($n = 8, 10\ldots$) are related to the eigenvectors of the previous eigenvectors by a reflection around the x axis and hence are not plotted. A polar representation is given in the Appendix A 3.

correlations and temperature in this basis as a Fourier series we get

$$\begin{aligned}\mathcal{C}_r(x,y,\tau) &= \hat{A}_0(x,\tau) + \sum_{n=1} \hat{A}_n^+(x,\tau)\phi_n^+(y) \\ &\quad + \hat{A}_n^-(x,\tau)\phi_n^-(y), \\ \mathcal{T}(y,\tau) &= \hat{T}_0(\tau) + \sum_{n=1} \hat{T}_n^+(\tau)\phi_n^+(y) + \hat{T}_n^-(\tau)\phi_n^-(y),\end{aligned} \tag{50}$$

where $\hat{A}_n^{\pm}(x,\tau) = \int_0^L \mathcal{C}_r(x,y,\tau)\phi_n^{\pm}(y)dy$, $\hat{A}_0(x,\tau) = \int_0^L \mathcal{C}_r(x,y,\tau)\phi_0 dy$, $\hat{T}_n^{\pm}(\tau) = \int_0^L \mathcal{T}_r(y,\tau)\phi_n^{\pm}(y)dy$, $\hat{T}_0(\tau) = \int_0^L \mathcal{T}_r(y,\tau)\phi_0 dy$. Using these expressions in the PDEs (see Appendix A 2) we get

$$\dot{\hat{T}}_0 = 0,\ \dot{\hat{T}}_n^{\mp} = -\tfrac{1}{\sqrt{2\gamma}}(1 \pm i)\lambda_n^{3/4}\hat{T}_n^{\mp},\ \ n = 1, 2, 3\ldots \tag{51}$$

where $\lambda_n = (n\pi/L)^2$. This can be interpreted in domain $y \in [0, L]$ as

$$\begin{aligned}\partial_\tau \mathcal{T}_r(y,\tau) &= -\frac{1}{\sqrt{2\gamma}}(|\Delta|^{3/4} - \nabla|\Delta|^{1/4})\mathcal{T}_r(y,\tau), \\ &= -\frac{1}{\sqrt{2\gamma}}\mathbb{L}_\infty \mathcal{T}_r(y,\tau),\end{aligned} \tag{52}$$

where $\mathbb{L}_\infty$ is a positive operator defined by its action as $\mathbb{L}_\infty \phi_n^{\pm}(y) = \lambda_n^{3/4}[1 - i\ \mathrm{sgn}(n)]\phi_n^{\pm}(y)$. With $L \to \infty$ the spectrum becomes continuous and the eigenfunctions become plane wave. Thus in for an infinite system at equilibrium, evolution of the temperature profile is given by a skew-symmetric fractional Laplacian given in Eq. (3) of the main text.

One can alternatively see this equivalence from the integrodifferential evolution in infinite space through the action of the operator $\partial_\tau T(y,\tau) = -\frac{1}{\sqrt{2\gamma}}\mathbb{L}_\infty T(y,\tau)$. A similar calculation as in Sec. III D gives

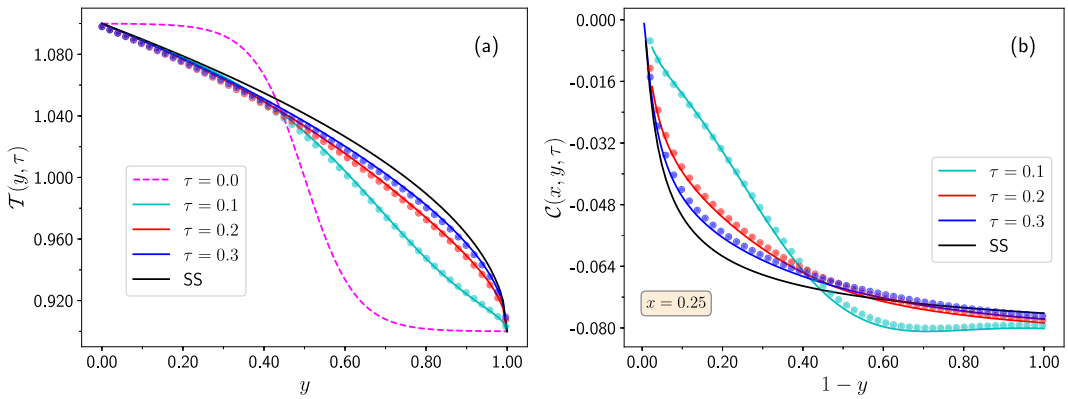

FIG. 5. Numerical verification of the evolution of (a) temperature profiles $\mathcal{T}(y,\tau) = \mathcal{T}_{ss}(y) + \mathcal{T}_r(1-y,\tau)$ obtained using the solution of Eq. (13). (b) The correlation $\mathcal{C}(x,y,\tau) = \mathcal{C}_{ss}(x,y) + \mathcal{C}_r(x,1-y,\tau)$ given in Eq. (10), where $\mathcal{C}_r$ is computed using the solution in Eq. (12). The magenta dashed line and the solid black line represent the initial and the NESS temperature profiles, respectively. Symbols are obtained from simulations with $\lambda = \gamma = 1$, $T_\ell = 1.1$, $T_r = 0.9$, and $L = 2048$, and the solid lines are from theory.

$\mathbb{L}_\infty f(y) = \frac{1}{\sqrt{\pi\gamma}}\,\partial_y \int_{-\infty}^{y} \frac{\partial_{y'} f(y')}{\sqrt{y-y'}} dy'$, where in contrast to (45), the lower limit is changed from $-\infty$ to 0. Using the identity

$$\int_{-\infty}^{y} dz \frac{1}{\sqrt{y-z}}\, e^{iqz} = \frac{\sqrt{\pi}}{\sqrt{iq}}\, e^{iqy},$$

one can easily show that

$$\mathbb{L}_\infty\, e^{iqy} = \lambda_q\, e^{iqy}, \quad \lambda_q = \sqrt{\frac{1}{2\gamma}}[1 - i\ \mathrm{sgn}(q)]\ |q|^{3/2},$$

which is same as the Fourier spectrum of the skew-symmetric fractional Laplacian given in Eq. (3) of the main text.

IV. CONCLUSION

In this paper, we have studied anomalous transport in a one-dimensional system with two conserved quantities in the open system setup. Starting from a microscopic description and acquiring knowledge about scaling properties from numerical studies, we derive exact expressions of the temperature profiles and the two-point correlations in the steady state. We also study the evolution of these quantities towards steady state. We explicitly show that the evolution of the temperature profiles in this model is governed by a nonlocal operator defined inside a finite domain which correctly takes the previously obtained infinite system representation. We provide numerical verifications of the analytical results. Our work provides the first clear and transparent microscopic derivation of a nonlocal heat equation describing anomalous transport in finite geometry and its connection to the corresponding skew-fractional equation in the infinite domain.

ACKNOWLEDGMENTS

We thank C. Bernardin, C. Mejía-Monasterio, S. Olla, and S. Lepri for very useful discussions. A.K. acknowledges support from a DST grant under Project No. ECR/2017/000634. This work benefited from the support of Project EDNHS ANR-14-CE25-0011 of the French National Research Agency (ANR) and of the Project 5604-2 of the Indo-French Centre for the Promotion of Advanced Research (IFCPAR).

APPENDIX

1. Boundary equations

The dynamical equations at the boundaries are given by

1. For $i = j = 1$

$$\dot{T}_1 = 2\lambda T_\ell + 2C_{1,2} - 2\lambda T_1 + \gamma[T_2 - T_1] \tag{A1}$$

2. For $i = j = L$

$$\dot{T}_L = 2\lambda T_r - 2C_{L-1,L} - 2\lambda T_L + \gamma[T_{L-1} - T_L] \tag{A2}$$

3. $i = 1$ and $2 < j < L$

$$\dot{C}_{1,j} = C_{2,j} - \lambda C_{1,j} + C_{1,j+1} - C_{1,j-1} + \gamma[C_{1,j-1} + C_{1,j+1} + C_{2,j} - 3C_{1,j}] \tag{A3}$$

4. $j = L$ and $1 < i < L - 1$

$$\dot{C}_{i,L} = C_{i+1,L} - C_{i-1,L} - C_{i,L-1} - \lambda C_{i,L} + \gamma[C_{i-1,L} + C_{i+1,L} + C_{i,L-1} - 3C_{i,L}] \tag{A4}$$

5. $i = 1$ and $j = L$

$$\dot{C}_{1,L} = C_{2,L} - C_{1,L-1} - 2\lambda C_{1,L} + \gamma[C_{2,L} + C_{1,L-1} - 2C_{1,L}] \tag{A5}$$

6. $i = 1$ and $j = 2$

$$\dot{C}_{1,2} = T_2 - \lambda C_{1,2} + C_{1,3} - T_1 + \gamma[C_{1,3} - C_{1,2}] \tag{A6}$$

7. $j = L$ and $i = L - 1$

$$\dot{C}_{L-1,L} = T_L - C_{L-2,L} - T_{L-1} - \lambda C_{L-1,L} + \gamma[C_{L-2,L} - C_{L-1,L}] \tag{A7}$$

2. Fractional equation in infinite domain

The expansions in the main text Eq. (50) along with the set of PDEs Eq. (6)–(8) gives the following differential equation

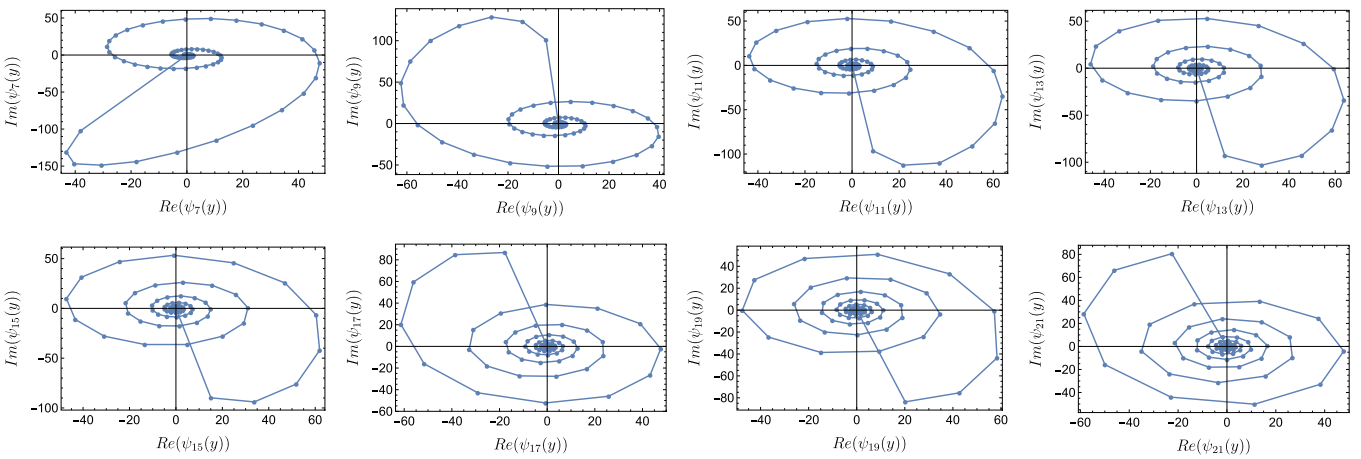

FIG. 6. Polar plots showing the real and imaginary parts of the eigenvectors for $n \geqslant 7$. The polar plots are for $n = 7, 9, 11 \ldots$.

for the components:

$$\partial_x^2 \hat{A}_n^{\pm}(x,\tau) = [(1 \mp i)\alpha_n]^2 \hat{A}_n^{\pm}(x,\tau),\ \partial_x^2 \hat{A}_0(x,\tau) = 0,$$
$$\pm \frac{in\pi}{L} \hat{T}_n^{\pm}(\tau) = -2\gamma \partial_x \hat{A}_n^{\pm}(x,\tau)_{|x\to 0}, \quad \text{(A8)}$$

where $\alpha_n = \sqrt{\frac{n\pi}{2L\gamma}}$. The solutions to these equations are in general given as $\hat{A}_n^{\pm}(x,\tau) = a_n^{\pm}(\tau) e^{\pm\alpha_n(1\mp i)x}$, $\hat{A}_0(x,\tau) = d(\tau)x + e(\tau)$. Choosing solutions which do not blow up at infinity at large x and obey the boundary conditions, we have $\mathcal{C}_r(x,y,\tau) = e(\tau) + \sum_{n=1}^{\infty} a_n^- e^{-\alpha_n(1+i)x} \phi_n^-(y) + \text{c.c.}$, where c.c. stands for complex conjugate. $e(\tau)$ is zero because there is no time-dependent source in the system. Using the above equations, we have

$$\hat{T}_n^{\pm} = 2\gamma a_n^{\mp}(\tau)\alpha_n \frac{(1 \mp i)}{(n\pi/L)}, \quad \dot{\hat{T}}_n^{\mp} = \mp 2i \frac{n\pi}{L} a_n^{\pm}(\tau). \quad \text{(A9)}$$

Using these two, we have Eq. (51) of the main text.

3. Polar plots of eigenvectors

The polar plots for eigenvectors of **B** are given in Fig. 6.

[1] O. Narayan and S. Ramaswamy, Anomalous Heat Conduction in One-Dimensional Momentum-Conserving Systems, Phys. Rev. Lett. **89**, 200601 (2002).

[2] H. Van Beijeren, Exact Results for Anomalous Transport in One-Dimensional Hamiltonian Systems, Phys. Rev. Lett. **108**, 180601 (2012).

[3] H. Spohn, Nonlinear fluctuating hydrodynamics for anharmonic chains, J. Stat. Phys. **154**, 1191 (2014).

[4] V. Lee, C. H. Wu, Z. X. Lou, Wei Li Lee, and C. W. Chang, Divergent and Ultrahigh Thermal Conductivity in Millimeter-Long Nanotubes, Phys. Rev. Lett. **118**, 135901 (2017).

[5] S. Lepri, R. Livi, and A. Politi, Universality of anomalous one-dimensional heat conductivity, Phys. Rev. E **68**, 067102 (2003).

[6] A. Dhar, Heat transport in low-dimensional systems, Adv. Phys. **57**, 457 (2008).

[7] S. Lepri, R. Livi, and A. Politi, Heat transport in low dimensions: Introduction and phenomenology, Lect. Notes Phys. **921**, 1 (2016).

[8] A. Dhar, Heat Conduction in a One-Dimensional Gas of Elastically Colliding Particles of Unequal Masses, Phys. Rev. Lett. **86**, 3554 (2001).

[9] S. Lepri, R. Livi, and A. Politi, On the anomalous thermal conductivity of one-dimensional lattices, Europhys. Lett. **43**, 271 (1998).

[10] S. Liu, P. Hänggi, N. Li, J. Ren, and Baowen Li, Anomalous Heat Diffusion, Phys. Rev. Lett. **112**, 040601 (2014).

[11] S. G. Das, A. Dhar, and O. Narayan, Heat conduction in the α-β Fermi-Pasta-Ulam chain, J. Stat. Phys. **154**, 1 (2014).

[12] C. Bernardin, P. Gonçalves, M. Jara, M. Sasada, and M. Simon, From normal diffusion to superdiffusion of energy in the evanescent flip noise limit, J. Stat. Phys. **159**, 1327 (2015).

[13] C. Bernardin and G. Stoltz, Anomalous diffusion for a class of systems with two conserved quantities, Nonlinearity **25**, 1099 (2012).

[14] M. Jara, T. Komorowski, and S. Olla, Superdiffusion of energy in a chain of harmonic oscillators with noise, Commun. Math. Phys. **339**, 407 (2015).

[15] Y. Hong, C. Zhu, M. Ju, J. Zhang, and X. C. Zeng, Lateral and flexural phonon thermal transport in graphene and stanene bilayers, Phys. Chem. Chem. Phys. **19**, 6554 (2017).

[16] X. Xu, L. F. C. Pereira, Yu. Wang, J. Wu, K. Zhang, X. Zhao, S. Bae, C. T. Bui, R. Xie, J. T. L. Thong *et al.*, Length-dependent thermal conductivity in suspended single-layer graphene, Nat. Commun. **5**, 3689 (2014).

[17] E. Lotfi, M. Neek-Amal, and M. Elahi, Molecular dynamics simulation of temperature profile in partially hydrogenated graphene and graphene with grain boundary, J. Mol. Graphics Modell. **62**, 38 (2015).

[18] D. A. Kessler and E. Barkai, Theory of Fractional Lévy Kinetics for Cold Atoms Diffusing in Optical Lattices, Phys. Rev. Lett. **108**, 230602 (2012).

[19] Y. Sagi, M. Brook, I. Almog, and N. Davidson, Observation of Anomalous Diffusion and Fractional Self-Similarity in One Dimension, Phys. Rev. Lett. **108**, 093002 (2012).

[20] G. M. Viswanathan, V. Afanasyev, S. V. Buldyrev, E. J. Murphy, P. A. Prince, and H. E. Stanley, Nature (London) **381**, 413 (1996).

[21] S. V. Buldyrev, S. Havlin, A. Ya Kazakov, M. G. E. Da Luz, E. P. Raposo, H. E. Stanley, and G. M. Viswanathan, Average time spent by Lévy flights and walks on an interval with absorbing boundaries, Phys. Rev. E **64**, 041108 (2001).

[22] I. Bronstein, Y. Israel, E. Kepten, S. Mai, Y. Shav-Tal, E. Barkai, and Y. Garini, Transient Anomalous Diffusion of Telomeres in the Nucleus of Mammalian Cells, Phys. Rev. Lett. **103**, 018102 (2009).

[23] J.-H. Jeon, V. Tejedor, S. Burov, E. Barkai, C. Selhuber-Unkel, K. Berg-Sørensen, L. Oddershede, and R. Metzler, In Vivo Anomalous Diffusion and Weak Ergodicity Breaking of Lipid Granules, Phys. Rev. Lett. **106**, 048103 (2011).

[24] P. Barthelemy, J. Bertolotti, and D. S. Wiersma, A Lévy flight for light, Nature (London) **453**, 7194 (2008).

[25] N. Mercadier, W. Guerin, M. Chevrollier, and R. Kaiser, Lévy flights of photons in hot atomic vapours, Nat. Phys. **5**, 602 (2009).

[26] D. Sierociuk, A. Dzieliński, G. Sarwas, I. Petras, I. Podlubny, and T. Skovranek, Modelling heat transfer in heterogeneous media using fractional calculus, Philos. Trans. R. Soc. London A **371**, 1990 (2013).

[27] X.-J. Yang and D. Baleanu, Fractal heat conduction problem solved by local fractional variation iteration method, Therm. Sci. **17.2**, 625 (2013).

[28] Amr M. S. Mohammed, Y. R. Koh, B. Vermeersch, H. Lu, P. G. Burke, A. C. Gossard, and A. Shakouri, Fractal Lévy heat transport in nanoparticle embedded semiconductor alloys, Nano Lett. **15**, 4269 (2015).

[29] H. Spohn, Fluctuating hydrodynamics approach to equilibrium time correlations for anharmonic chains, Lect. Notes Phys. **921**, 107 (2016).

[30] C. B. Mendl and H. Spohn, Current fluctuations for anharmonic chains in thermal equilibrium, J. Stat. Mech. (2015) P03007.

[31] G. Basile, C. Bernardin, and S. Olla, Momentum Conserving Model with Anomalous Thermal Conductivity in Low Dimensional Systems, Phys. Rev. Lett. **96**, 204303 (2006).

[32] C. Bernardin, P. Gonçalves, and M. Jara, 3/4-Fractional superdiffusion in a system of harmonic oscillators perturbed by a conservative noise, Arch. Ration. Mech. Anal. **220**, 505 (2016).

[33] Fractional Laplacian, 2018, https://www.ma.utexas.edu/mediawiki/index.php/Fractional_Laplacian.

[34] Fractional heat equation, 2012, https://www.ma.utexas.edu/mediawiki/index.php/Fractional_heat_equation.

[35] G. M. Viswanathan, V. Afanasyev, Sergey V. Buldyrev, Shlomo Havlin, M. G. E. Da Luz, E. P. Raposo, and H. Eugene Stanley, Levy flights in random searches, Phys. A (Amsterdam, Neth.) **282**, 1 (2000).

[36] A. Zoia, A. Rosso, and M. Kardar, Fractional Laplacian in bounded domains, Phys. Rev. E **76**, 021116 (2007).

[37] S. Lepri, C. Mejía-Monasterio, and A. Politi, A stochastic model of anomalous heat transport: Analytical solution of the steady state, J. Phys. A: Math. Theor. **42**, 025001 (2009).

[38] L. Delfini, S. Lepri, R. Livi, and A. Politi, Nonequilibrium Invariant Measure Under Heat Flow, Phys. Rev. Lett. **101**, 120604 (2008).

[39] J. Cividini, A. Kundu, A. Miron, and D. Mukamel, Temperature profile and boundary conditions in an anomalous heat transport model, J. Stat. Mech. (2017) 013203.

[40] S. Lepri, C. Mejía-Monasterio, and A. Politi, Nonequilibrium dynamics of a stochastic model of anomalous heat transport, J. Phys. A: Math. Theor. **43**, 065002 (2010).

[41] S. Lepri and A. Politi, Density profiles in open superdiffusive systems, Phys. Rev. E **83**, 030107(R) (2011).